

# Systematic characterization of the tumor microenvironment in Chinese patients with hepatocellular carcinoma highlights intratumoral B cells as a potential immunotherapy target

YU FENG<sup>1\*</sup>, LIGUO LIU<sup>2\*</sup>, JING LI<sup>1</sup>, JIA HUANG<sup>2</sup>, JENNY H. XIE<sup>3</sup>, LAURENCE MENARD<sup>3</sup>, YANFEN SHI<sup>4</sup>, XIAOHONG ZHAO<sup>1</sup>, SHAN XIE<sup>1</sup>, WENJUAN ZANG<sup>1</sup>, HAIDONG TAN<sup>2</sup>, ZHIYING YANG<sup>2</sup> and LING NI<sup>1,5</sup>

<sup>1</sup>Institute for Immunology and School of Medicine, Tsinghua University, Beijing 100084;

<sup>2</sup>Department of Hepatobiliary Surgery, China-Japan Friendship Hospital, Beijing 100029, P.R. China;

<sup>3</sup>Research and Early Development, Bristol Myers Squibb, Princeton, NJ 08540, USA;

<sup>4</sup>Department of Pathology, China-Japan Friendship Hospital, Beijing 100029;

<sup>5</sup>Center for Human Disease Immuno-monitoring, Beijing Friendship Hospital, Beijing 100050, P.R. China

Received August 3, 2021; Accepted December 1, 2021

DOI: 10.3892/or.2021.8249

**Abstract.** Hepatocellular carcinoma (HCC) is an immunogenic malignancy, which exhibits low responsiveness to programmed cell death protein-1 (PD-1)/programmed death ligand-1 (PD-L1) antibodies. Therefore, the identification of novel immunotherapeutic targets to treat HCC is imperative. Systematic characterization of the HCC tumor microenvironment (TME) can provide novel insight into additional therapeutic approaches. In the present study, the RNA-sequencing (RNA-seq) data of 360 patients with HCC were integrated from The Cancer Genome Atlas to assess the expression of membrane spanning 4-domains A1 (*MS4A1*; encoding CD20) in tumors and normal liver tissues. Immunofluorescence and multiplex tissue fluorescence analyses

were performed and combined with flow cytometry staining to measure CD20/CD19 expression at the protein level. In addition, published single cell RNA-seq data of CD45<sup>+</sup> cells were derived from 16 treatment-naïve patients from Beijing Shijitan Hospital with HCC to illustrate the characteristics of CD19<sup>+</sup> B cells. The results indicated that the HCC TME included nuclear receptor subfamily 4 group A member 2<sup>+</sup> (NR4A2) B cells. Patients with HCC and high density of intratumoral B cells demonstrated compromised antitumor immunity manifested by low percentages of cytotoxic CD8<sup>+</sup> T cells and high density of regulatory T cells. Furthermore, PD-L1 expression was significantly correlated with the B cell signature marker CD20. The present study indicated that tumor-infiltrating B cells may play a negative role in antitumor immunity and serve as a promising target for HCC immunotherapy, alone or in combination with anti-PD-L1/PD-1 antibodies.

*Correspondence to:* Dr Ling Ni, Institute for Immunology and School of Medicine, Tsinghua University, 30 Haidian Shuangqing Road, Beijing 100084, P.R. China  
E-mail: lingni@tsinghua.edu.cn

Dr Zhiying Yang, Department of Hepatobiliary Surgery, China-Japan Friendship Hospital, Sakura Garden East Street, Beijing 100029, P.R. China  
E-mail: yangzhy@aliyun.com

\*Contributed equally

**Abbreviations:** HCC, hepatocellular carcinoma; AFP,  $\alpha$ -fetoprotein; TME, tumor microenvironment; TCGA, The Cancer Genome Atlas; B-TILs, tumor-infiltrating B cells; CTLs, cytotoxic CD8<sup>+</sup> T cells; Breg cells, regulatory B cells; TLS, tertiary lymphoid structure; ICB, immune checkpoint blockade; PBMCs, peripheral blood mononuclear cells; UMAP, non-linear dimensional reduction

**Key words:** hepatocellular carcinoma, HCC, B cells, antitumor immunity, immunotherapy, programmed cell death protein-1/programmed death ligand-1

## Introduction

Liver cancer is the fifth most common cancer type and the second most common cause of cancer-related mortality worldwide (1). Hepatocellular carcinoma (HCC) accounts for ~90% of primary liver cancers, and its incidence has been constantly increasing (2). In China, HCC has a higher incidence and may account for 50% of new cases globally each year (3). The majority of HCC cases in China and southeastern Asia are caused by hepatitis B virus (HBV) infection, while non-alcoholic-associated steatosis may be one of the main causes of the development of HCC in Western countries (4). In the early stages, liver transplantation or hepatic resection is the standard treatment approach, with a high probability of recurrence-free postoperative course, while in advanced or metastatic stages, sorafenib (a broad tyrosine kinase inhibitor) is typically used (5). HCC is an immunogenic tumor that occurs in chronically inflamed livers (6). Therapeutic antibodies blocking the programmed cell death protein-1 (PD-1)/programmed death ligand-1 (PD-L1) interaction were approved by the Food and Drug Administration to treat advanced HCC in patients

previously treated with sorafenib as a second line treatment (7). However, the observed objective response rate was not impressive (~20%) in response to PD-1/PD-L1 antibody treatment (8). Therefore, the identification of novel immunotherapeutic targets in advanced HCC is imperative.

The tumor microenvironment (TME) is widely used as a biomarker for the identification of novel therapeutic targets. The HCC TME consists of cancer and stromal cells, including hepatic stellate cells, cancer-associated fibroblasts, immune cells and endothelial cells, which interact with the tumor and affect its growth (9). The role of tumor-infiltrating B cells (B-TILs) remains controversial. Shalpour *et al* (10) indicated that immunoglobulin (Ig) A-expressing B cells could elicit depletion of liver cytotoxic CD8<sup>+</sup> T cells (CTLs) and that IgA<sup>+</sup> cell depletion could enhance the regression of established non-alcoholic-associated steatosis-induced HCC. Furthermore, it was also shown that a high number of T cell Ig and mucin domain-1<sup>+</sup> regulatory B (Breg) cells could infiltrate into the tumors of patients with HCC (11,12). These infiltrating Breg cells were found to express IL-10 and demonstrate high suppressive activity against T cells. Mechanistically, the CD40/CD154 signaling pathway was found to be involved in HCC progression via the activation of Breg cells (13,14). By contrast, Zhang *et al* (15) demonstrated that B cell infiltration into tumors was significantly impaired during tumor progression, whereas high density of B-TILs correlated with improved clinical outcome. Moreover, the expression levels of CD19 and CD38 were positively correlated with HCC patient survival (16). Recent studies have shown that B cells are a vital fraction in the formation of tertiary lymphoid structures (TLSs). The presence of TLSs in patients is associated with an improved clinical response to the immune checkpoint blockade in melanoma, sarcoma and renal cell carcinoma tumors (17-19). However, to the best of our knowledge, the clinical significance and functions of B-TILs in Chinese patients with HCC have not been previously reported. The investigation of these topics is of high importance for HCC immunotherapy.

In the present study, clinical specimens were collected from patients with HCC in Beijing. The clinical data and the function of B-TILs were assessed. Following immunofluorescence (IF) staining, it was found that HCC tumors were highly enriched with CD19/CD20<sup>+</sup> B cells, which was associated with compromised cytotoxic function of T and natural killer (NK) cells. In addition, PD-L1 expression correlated significantly with CD20 expression. Collectively, these findings indicate that B-TILs may be a promising candidate for HCC immunotherapy, alone or in combination with anti-PD-L1/PD-1 antibodies.

## Materials and methods

**Patients and specimens.** Fresh tumor tissues, para-tumor tissues, normal liver and matched blood samples were collected from patients with HCC undergoing surgical treatment at the China-Japan Friendship Hospital (Beijing, China). From May 2018 to July 2020, 50 patients were enrolled in this study. The ratio of male to female patients was 42:8. The mean age was 60.8 years, with an age range from 36 to 84 years. All patient data were anonymized prior to study inclusion.

All procedures followed were in accordance with the ethical standards of the responsible committee on human

experimentation (The Institutional Review Board at Tsinghua University (Beijing, China) and with the Helsinki Declaration of 1975, as revised in 2000 (5). All studies were approved by the Medical Ethics Committee at Tsinghua University (approval no. 20180017). Informed consent was obtained from all the subjects in this study.

**Isolation of peripheral blood mononuclear cells (PBMCs) and tumor-infiltrating lymphocytes (TILs).** Blood samples from patients with HCC were incubated in heparinized tubes and centrifuged on Ficoll-Hypaque gradients (Cytiva). Fresh normal liver, para-tumor and tumor samples from patients with HCC were digested in RPMI-1640 medium (Gibco; Thermo Fisher Scientific, Inc.) supplemented with 0.5 mg/ml Collagenase Type IV (Gibco; Thermo Fisher Scientific, Inc.), 10% FBS (Gibco; Thermo Fisher Scientific, Inc.) plus 10 U/ml DNase I for 30 min at 37°C prior to Ficoll-Hypaque (Cytiva) gradient centrifugation.

**Flow cytometry.** The following antibodies were used: Anti-CD45 (cat. no. HI30; eBioscience™), anti-CD19 (cat. no. HIB19, eBioscience™), anti-CD3 (cat. no. OKT3 OKT3), anti-CD56 (cat. no. HCD56; BioLegend), anti-CD8 (cat. no. SK1; BD Biosciences), anti-interferon  $\gamma$  (IFN- $\gamma$ ; cat. no. B27; BioLegend), anti-tumor necrosis factor- $\alpha$  (TNF- $\alpha$ ; cat. no. MAb11; Invitrogen™; Thermo Fisher Scientific, Inc.), anti-Ki67 (cat. no. B56; BD Biosciences), anti-ranzyme B (cat. no. GRB05; Thermo Fisher Scientific, Inc.) and anti-perforin (cat. no. dG9; Thermo Fisher Scientific, Inc.). The cells were stimulated with phorbol 12-myristate 13-acetate (50 ng/ml; Sigma-Aldrich; Merck KGaA) and ionomycin (500 ng/ml; Sigma-Aldrich; Merck KGaA) for 1 h and subsequently Brefeldin A (Golgi-plug; BD Biosciences) was added for an additional 4 h. Single cell suspensions were stained with antibodies against surface molecules at 4°C for 20 min. Intracellular cytokine staining was performed following fixation of the cells and their permeabilization with eBioscience Fixation/Permeabilization buffer. Finally, the cells were stained with antibodies at 4°C for 40 min. The cells were analyzed on a LSR Fortessa (BD Biosciences) flow cytometer and the data were analyzed using FlowJo.X 10.8 software (FlowJo, LLC). The non-viable cells were excluded based on viability dye staining (Fixable viability dye eF506; eBioscience; Thermo Fisher Scientific, Inc.).

**Histological and immunohistochemical analyses.** All samples were fixed with 4% neutral formaldehyde, dehydrated conventionally and embedded in paraffin. The slides were cut at a thickness of 4  $\mu$ m, stained with hematoxylin and eosin (H&E) and observed under light microscopy. Immunohistochemical staining was performed using the streptavidin-peroxidase method. The primary antibodies [anti- $\alpha$ -fetoprotein (AFP), anti-Ki67 and anti-CD34] and other kits were purchased from Beijing Zhongshan Jinqiao Biotechnology Co., Ltd.; OriGene Technologies, Inc. All operating procedures were carried out in strict accordance with the instructions provided by the manufacturer. PBS buffer was used instead of the primary antibody as negative control and the known positive specimens were used as positive control.

**IF and multiplex tissue fluorescence.** All samples were fixed in formalin solution and embedded in paraffin. The IF activity was performed according to the method described previously (20). Each slide was incubated with the primary antibodies against CD45 (cat. no. ab10559; Abcam), CD20 (cat. no. ab9475; Abcam), CD138 (cat. no. ab34164; Abcam) or PD-L1 (cat. no. ab58810, Abcam) at 4°C overnight. AffiniPure F(ab')<sub>2</sub> Fragment donkey anti-rabbit/mouse/goat Ig was selected as the secondary antibody. The slides were incubated with mounting medium containing DAPI for 20 min. The images were obtained using a fluorescence microscope (Carl Zeiss AG). The quantification analysis was performed using ImageJ 1.51p (National Institutes of Health) software. Multiplex tissue fluorescence staining was performed following blocking with the blocking buffer for 15 min and each slide was incubated with the primary antibodies against CD20 (cat. no. ab9475; Abcam), CD56 (cat. no. ab200698; Abcam), CD4 (cat. no. ab133616, Abcam), CD8 (cat. no. ab199016; Abcam) and forkhead box P3 (FOXP3; cat. no. ab20034; Abcam) at 4°C overnight. Anti-mouse/rabbit HRP was used as the secondary antibody. The images were acquired by Vectra Polaris 1.0.7 and analyzed by inform 2.4.1 (Perkin Elmer, Inc.).

**Single cell sequencing data analysis.** 10x Genomics data were downloaded from the Gene Expression Omnibus (GSE) dataset GSE140228 (21). The immune cells in tumors and PBMCs were separated for further analysis. Seurat (21) was used to perform clustering analysis of single-cell data from different tissues. The cells that exhibited unique feature counts over 6,000 or <200 were filtered. The cells that exhibited <10% mitochondrial genes, and genes expressed in >3 cells were selected for further analysis. The datasets from different tissues were integrated together using the FindIntegrationAnchors and IntegrateData function.

Non-linear dimensional reduction (UMAP) (22) was selected for clustering analysis. B cells were selected for this analysis. FindMarkers function was performed to identify differentially expressed markers across tissues. FeaturePlot function was used to visualize the gene expression changes with the split by option.

**Statistical analysis.** Statistical comparisons were performed using unpaired Student's t-test for two-group analysis or ordinary One-way ANOVA followed by Dunnett's multiple comparison test for three-group analysis. Simple linear regression was used to calculate the correlations.  $P < 0.05$  was considered to indicate a statistically significant difference.

## Results

**HCC tumors are enriched by CD20<sup>+</sup> B cells and CD45<sup>+</sup>CD138<sup>+</sup> plasma cells.** To explore the roles of B cells derived from HCC TME in tumor progression, the expression levels of membrane spanning 4-domains A1 (*MS4A1*; encoding CD20) were initially investigated using the online database The Cancer Genome Atlas. The data indicated that *MS4A1* expression in tumor tissues was decreased compared with that in normal control tissues (left panel, Fig. 1A). This result was further confirmed by investigation of the HCC tumor samples collected from the China-Japan Friendship

Hospital (right panel, Fig. 1A),  $n=14$  for normal tissue,  $n=34$  for paratumor and  $n=31$  for tumor. The tumors were stained with H&E for histological evaluation. Abnormalities in histopathological morphology were observed in all the cases examined (Fig. 1B). In total, 37.8% (17 of 45 cases) of the tumors were positive for AFP and 100% (41/41) for CD34. A high Ki67 index (>15%) was detected in 77.3% (34/44) of the cases. To note, some of the patients ( $N=50$ ) were not tested for AFP, CD34 or Ki67. The clinical and pathological characteristics of the treatment-naïve HCC patients are summarized in Table I.

Subsequently, IF was performed to assess CD20 protein levels in HCC tumor and control tissues. The expression levels of the CD20 protein were detected in normal ( $n=17$ ), para-tumor ( $n=46$ ) and tumor ( $n=50$ ) tissues (Fig. 2A and B). Non-significant differences were observed with regards to CD20 expression between normal and para-tumor tissues. However, in tumor tissues, the percentage of CD20<sup>+</sup> B cells was significantly elevated compared with that noted in the para-tumor tissues. The difference between normal controls and tumors was not statistically significant, which may be due to the smaller size of the normal control group (Fig. 2B). The low protein levels of CD20 in normal tissues were contradictory to the high mRNA levels noted in the same tissues, which suggested that translation of CD20 protein in these tissues may be restrictively regulated at the posttranscriptional or translation levels. Notably, no correlation was found between the density of CD20<sup>+</sup> B cells and the Ki67 score (data not shown).

In addition, the number of plasma cells in the HCC TME was measured (Fig. 2C). A significantly higher number of plasma cells (CD45<sup>+</sup>CD138<sup>+</sup> cells) were noted in the tumors than those found in the para-tumors or normal control samples. The majority of the patients did not exhibit plasma cells in either normal or para-tumor tissues, whereas these cells were present in the HCC tumors (Fig. 2C and D). Taken together, the data indicated that HCC tumors were infiltrated by CD20<sup>+</sup> B and CD45<sup>+</sup>CD138<sup>+</sup> plasma cells.

**Higher density of B-TILs is associated with compromised cytotoxic function of both T and NK cells.** In order to assess the clinical relevance of B-TILs, infiltrating lymphocytes were isolated from normal, para-tumor and tumor tissues and the percentage of B cells (CD3<sup>+</sup>CD19<sup>+</sup>) was analyzed via flow cytometry. The percentages of B cells were similar in the normal and para-tumor tissues and ranged from 0 to 10% of the total number of CD45<sup>+</sup> lymphocytes (Fig. 3A and B). In tumor tissues, nearly 50% of the patients indicated an increase in the percentage of CD19<sup>+</sup> B cells (1.6-38.8% of total CD45<sup>+</sup> lymphocytes), which was in line with the results derived from IF staining.

The patients were divided into two groups based on the B cell percentages of the total CD45<sup>+</sup> lymphocytes (the cut-off value was 1.5%), with 17 patients in the B cell<sup>high</sup> group and 19 patients in the B cell<sup>low</sup> group. The expression levels of the functional markers were analyzed in NK and T cells between the two groups. Although the frequency of CD3<sup>+</sup> TILs was significantly increased in the B cell<sup>high</sup> group, no significant difference was noted with regard to the percentage of NK cells (Fig. 3C). Subsequently, the functional capacities of these TILs were evaluated. Notably, the CD8<sup>+</sup> TILs in the B cell<sup>high</sup> group indicated reduced cytotoxic activity compared with

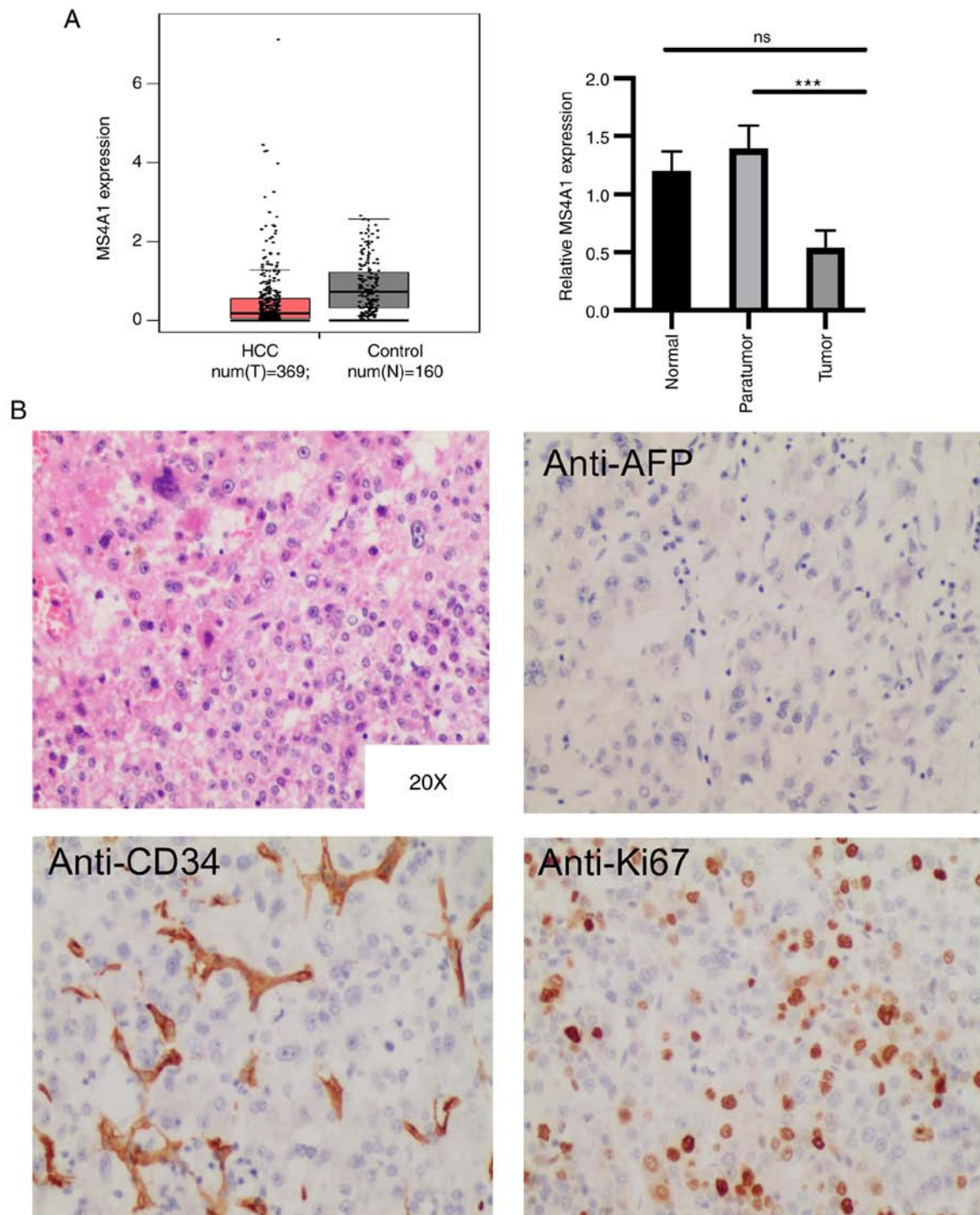


Figure 1. HCC tumors exhibit decreased levels of MS4A1 compared with those noted in the para-tumor samples. (A) (Left panel) Expression of MS4A1 in human HCC tumors (red) and normal control samples (gray) from the TCGA datasets. (Right panel) RT-qPCR analysis of *MS4A1* expression in normal (n=14), para-tumor (n=33) and tumor (n=31) tissues from treatment-naïve patients with HCC. The data are presented as mean  $\pm$  SEM. (B) Histological and immunohistochemical staining indicating abnormalities in histological morphology and in the expression levels of AFP, CD34 and Ki67 in the tumors. \*\*\* $P < 0.001$ ; ns, not significant. HCC, hepatocellular carcinoma; MS4A1, membrane spanning 4-domains A1; TCGA, The Cancer Genome Atlas; RT-qPCR, reverse-transcription quantitative PCR; SEM, standard error of the mean; AFP,  $\alpha$ -fetoprotein;

those in the B cell<sup>low</sup> group, based on the decreased expression levels of granzyme B, perforin and IFN- $\gamma$  (Fig. 3D) in the B cell<sup>high</sup> group. However, the cytotoxic activity of CD4<sup>+</sup> TILs was not significantly different between these two groups (data not shown). Moreover, non-significant differences were noted with regard to the tumor stage between the two groups (data not shown).

The concept of innate immunity is increasingly accepted in tumor immunology. NK cells act as innate effector lymphocytes that respond to tumor cells. The percentages of NK-TILs exhibited no significant differences between the B cell<sup>low</sup> and B cell<sup>high</sup> groups (Fig. 3E). In addition, the expression levels of perforin and granzyme B were not different between the two groups examined (Fig. 3E),

Table I. Clinicopathological features of the patients with HCC in this study.

Patient no.	Sex	Age (years)	HBV Positivity	BCLC stage	B-TIL density	Histochemistry		
						AFP	Ki67	CD34
1	Male	42	+	B	Low	+	40%	+
2	Male	65	-	A	High	-	10%+	+
3	Male	47	+	A	Low	NA	NA	+
4	Female	73	-	A	NA	-	30%	+
5	Male	73	+	A	Low	+	60%	+
6	Male	64	-	A	High	NA	NA	+
7	Male	36	+	C	Low	+	50%+	+
8	Male	62	-	A	High	-	30%+	NA
9	Female	59	+	A	High	+	NA	+
10	Male	58	+	C	High	-	50%+	+
11	Male	55	+	B	Low	+	20%+	+
12	Male	45	+	C	High	-	70%+	+
13	Male	51	+	B	High	-	60%+	+
14	Male	58	+	B	Low	+	90%+	+
15	Male	58	+	A	Low	-	40%+	+
16	Male	58	+	C	High	-	25%+	+
17	Male	65	+	C	High	-	80%+	+
18	Male	64	+	A	Low	-	60%+	+
19	Male	84	+	A	Low	-	10%	+
20	Male	72	+	A	Low	-	20%+	+
21	Male	81	-	C	Low	-	5%+	+
22	Male	77	-	B	High	+	60%+	+
23	Male	77	+	B	High	-	50%+	+
24	Female	60	+	A	Low	-	2%+	+
25	Male	60	+	B	High	-	5%+	+
26	Male	68	+	A	High	-	30%+	NA
27	Male	60	+	C	Low	-	30%+	+
28	Female	76	+	B	Low	NA	NA	+
29	Male	74	+	A	Low	+	30%+	+
30	Male	54	+	A	High	+	30%+	+
31	Male	61	+	A	High	-	30-40%+	+
32	Male	40	+	A	High	-	20%+	+
33	Male	66	+	B	Low	+	50%+	+
34	Male	63	+	B	High	-	20%+	NA
35	Male	46	+	A	High	-	20%+	+
36	Male	49	+	B	Low	+	70%+	+
37	Female	63	+	B	Low	+	40%+	NA
38	Male	63	+	A	Low	NA	NA	NA
39	Male	63	+	A	NA	-	15%+	+
40	Male	57	+	A	High	NA	NA	NA
41	Female	58	+	B	NA	+	60%+	+
42	Male	48	+	B	NA	-	5%+	+
43	Male	72	-	A	NA	+	60%+	+
44	Male	60	+	B	NA	+	60%+	+
45	Female	66	+	B	NA	+	10%+	+
46	Male	51	+	B	NA	+	60%+	NA
47	Male	76	+	A	NA	-	15%+	NA
48	Female	45	-	B	NA	-	5%+	NA
49	Male	47	+	A	NA	+	30%+	+
50	Male	70	+	B	NA	-	35%+	+

HCC, hepatocellular carcinoma; HBV, hepatitis B virus; BCLC, Barcelona clinic liver cancer; B-TILs, tumor-infiltrating B cells; AFP,  $\alpha$ -fetoprotein; NA, non-available.



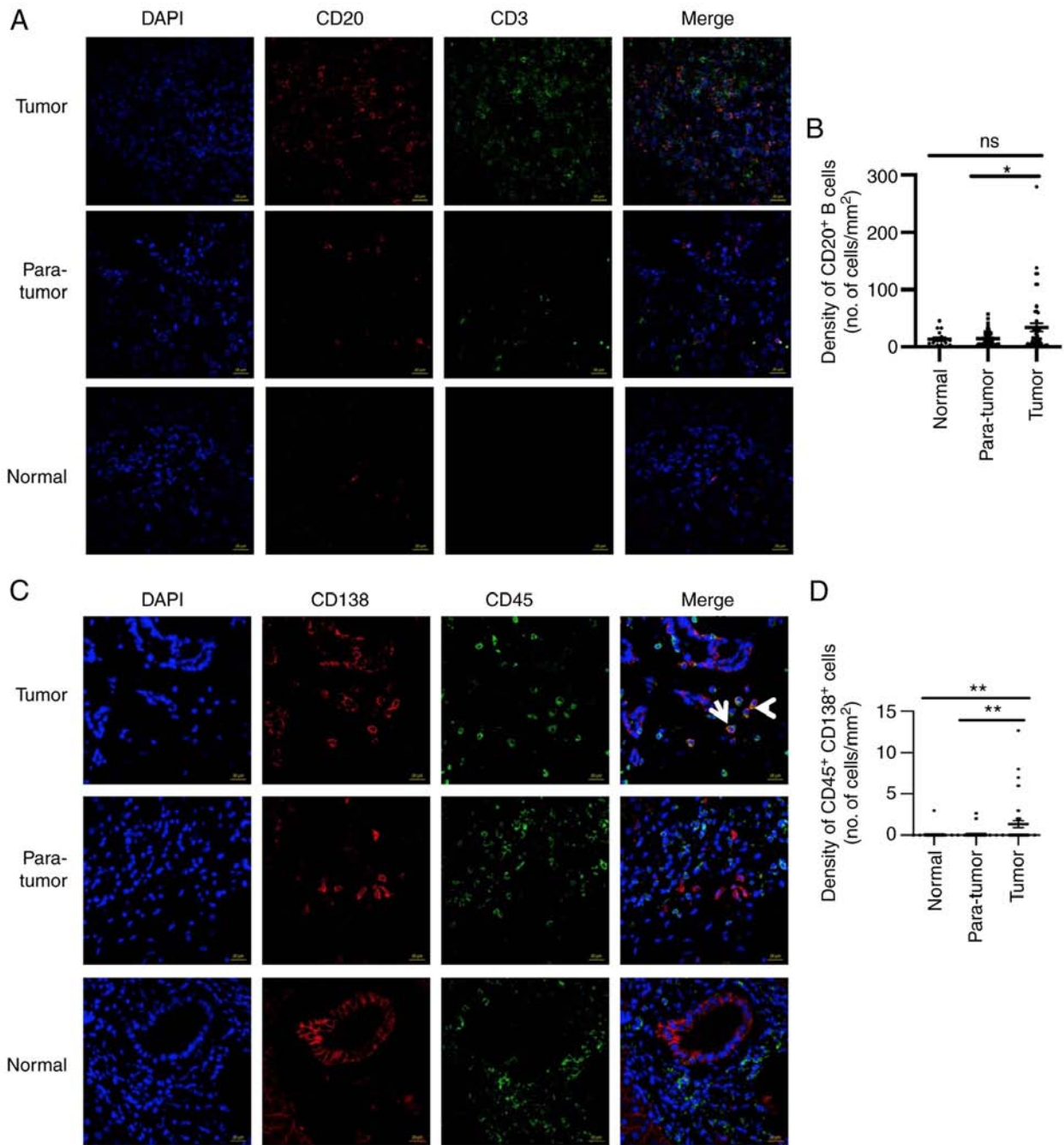


Figure 2. HCC tumors are enriched with CD20<sup>+</sup> B cells and CD45<sup>+</sup>CD138<sup>+</sup> plasma cells. (A) IF staining of CD20 and CD3 together with DAPI in paired tumors, para-tumor and normal control samples. (B) Quantification of CD20<sup>+</sup> B cell density (number of cells/mm<sup>2</sup>) in normal (n=17), para-tumor (n=46) and tumor (n=50) tissues by IF staining. (C) IF staining of CD138 (red) and CD45 (green) combined with DAPI in paired tumors, para-tumors and normal control samples. (D) Quantification of CD138<sup>+</sup>CD45<sup>+</sup> cell density (number of cells/mm<sup>2</sup>) in paired tumors (n=42), para-tumors (n=42) and normal control samples (n=42) by IF staining. \*P<0.05, \*\*P<0.01; ns, not significant. HCC, hepatocellular carcinoma; IF, immunofluorescence.

indicating that B cells did not affect NK cell function via the perforin/granzyme B pathway. However, the B cell<sup>high</sup> group indicated a significant decrease in the frequency of IFN- $\gamma$ <sup>+</sup>NK<sup>+</sup> cells, compared with that of the B cell<sup>low</sup> group (Fig. 3E). These results indicated that high accumulation of B cells in the TME was associated with reduced NK function in the TME.

*Intratumoral B cells are positively associated with infiltration of regulatory T cells (Treg) cells.* To further investigate the profile of immune cells in HCC tumors, multi-IF staining

was used to assess the colocalization of major lymphocyte subtypes identified by CD20, CD8, CD57, CD4 and FOXP3 in the tumor tissues from 38 patients with HCC. CD20<sup>+</sup> B cells were co-localized with both CD4<sup>+</sup> and CD8<sup>+</sup> T cells, while in some cases CD20<sup>+</sup> B cells were in contact with CD8<sup>+</sup> T cells (Fig. 4A). It was also shown that CD20<sup>+</sup> B cells were surrounded by CD8<sup>+</sup> T cells mostly in the stroma area. This was noted for 11 cases, which indicated the formation of TLS. It is interesting to note that FOXP3<sup>+</sup> Treg and CD20<sup>+</sup> B cells were closely colocalized within the TLS. In contrast to these observations, CD57<sup>+</sup> NK cells were not colocalized

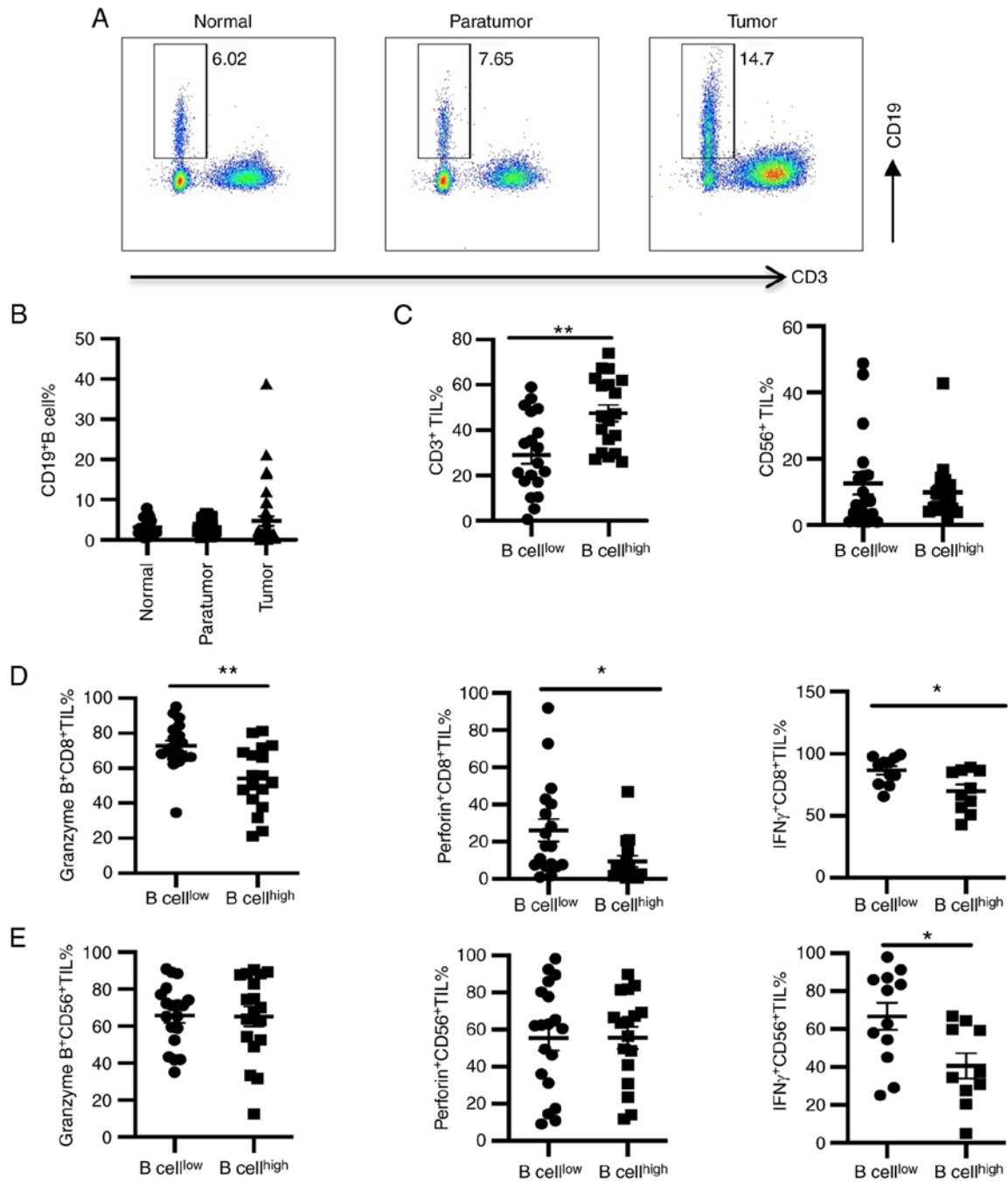


Figure 3. Increased intratumoral B cells are associated with compromised cytotoxic function of T and NK cells. (A) Representative FACS plots indicating CD3<sup>+</sup>CD19<sup>+</sup> B cell percentages in paired normal, para-tumor and tumor tissues. (B) Percentages of CD19<sup>+</sup> B cells across normal control, tumor and para-tumor samples. (C) Comparison of frequencies of lymphocyte subsets (CD3<sup>+</sup> TILs and CD56<sup>+</sup> TILs) between B cell<sup>high</sup> (% CD19<sup>+</sup> >1.5; n=19) and B cell<sup>low</sup> tumors (% CD19<sup>+</sup> <1.5; n=19). (D) Reduced granzyme expression and reduced percentages of B<sup>+</sup>CD8<sup>+</sup> TILs in the B cell<sup>high</sup> group (n=19) compared with those of the B<sup>low</sup> group (n=19). (E) Comparison of percentages of perforin<sup>+</sup>CD56<sup>+</sup> NK-TILs and IFN- $\gamma$ <sup>+</sup>CD56<sup>+</sup> NK-TILs in the B cell<sup>high</sup> (n=19) and B cell<sup>low</sup> (n=19) groups. \*P<0.05, \*\*P<0.01. NK, natural killer; FACS, fluorescence activated cell sorting; TILs, tumor-infiltrating lymphocytes; IFN- $\gamma$ , interferon  $\gamma$ .

with CD20<sup>+</sup> B cells (Fig. 4A). Additional quantification of the multi-IF staining data indicated that the number of CD20<sup>+</sup> B cells was positively correlated with FOXP3<sup>+</sup> Treg cells (Fig. 4B). In addition, the tumor tissues were divided into tumor bed and stroma areas. Statistical analysis indicated that the number of CD20<sup>+</sup> B cells was positively correlated with that of FOXP3<sup>+</sup> Treg cells in the tumor bed but not the stroma area (Fig. 4C and D), which indicated that B-TILs may contribute to the infiltration of Treg cells, which in turn leads to tumor immune escape.

*High levels of nuclear receptor subfamily 4 group A member 2 (NR4A2) are expressed in B-TILs.* To illustrate the characteristics of B cells in HCC, the present study used published single cell RNA-sequencing (RNA-seq) data of CD45<sup>+</sup> cells from 16 treatment-naïve patients with HCC (23). The single cell RNA-seq data of B cells from tumors and PBMCs were combined. UMAP was performed to identify three major clusters (C0, C1 and C2; Fig. 5A). The PBMCs contained 23% C0, 28% C1 and 49% C2, while the HCC tumors contained 80% C0, 15% C1 and 6% C2 (Fig. 5A). The C0 expressed markers

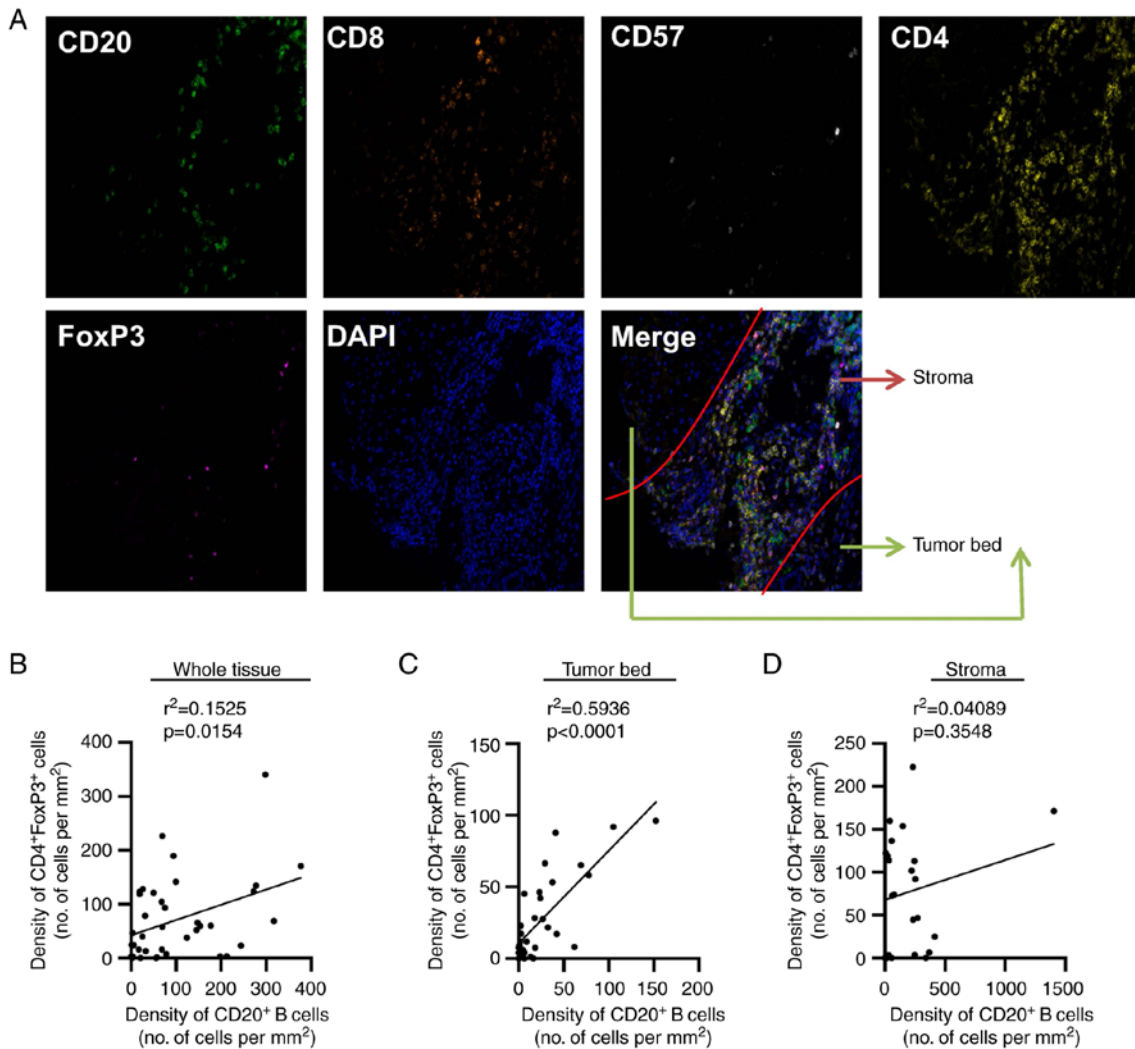


Figure 4. Intratumoral B cells are positively associated with infiltration of Treg cells. (A) Representative images from multiplex tissue fluorescence staining with DAPI (blue), CD20 (green), CD8 (orange), CD57 (white), CD4 (yellow) and FOXP3 (magenta) indicating a tertiary lymphoid structure. (B-D) Correlative analysis between the density of CD20<sup>+</sup> B cells and the density of CD4<sup>+</sup>FOXP3<sup>+</sup> cells, in whole tumors (B), tumor bed (C) and stroma (D), n=38. Treg, T regulatory cells; FOXP3, forkhead box P3.

of memory B cells, such as *CCL4*, *RGS2*, *AREG*, *ZFP36*, *CCL5*, *CD82* and *CD1C*, whereas the C1 expressed markers of plasmablasts, including *IGHG1*, *IGHG3*, *CD27*, *IGHG4*, *IGHA1*, *NEAT1*, *SSPN*, *S100A10* and *CPNE5*, and the C2 was mainly indicative of naïve B cells (*TCL1A*, *IGHD1*, *CD72*, *APLP2*, *CD200*, *GCA*, *CD79A*, *CD79B* and *CD74*; Fig. 5B). The expression levels of 17 genes (*FOS*, *RGS2*, *RGS1*, *CD83*, *CD69*, *JUNB*, *NR4A2*, *GPR183*, *HERPUD1*, *FOSB*, *YPEL5*, *SRGN*, *ANF331*, *IGHG1*, *ZFP36*, *SLC2A3* and *DUSP1*) were significantly increased in intratumoral B cells (fold change cut-off value >2) compared with those noted in peripheral B cells. Higher expression of *FOS*, *FOSB* and *JUNB*, which belong to the activator protein 1 (AP-1) pathway, were noted in HCC B-TILs than those noted in the peripheral B cells (Fig. 5C). In addition, NR4A2 expression was also enhanced in B-TILs (Fig. 5C). NR4A2 is a member of an orphan nuclear hormone receptor family involved in induction of apoptosis and carcinogenesis (24). It is preferentially recruited to the binding sites of the transcription factor AP-1, where it represses effector-gene expression by inhibiting AP-1 function in T cells (25,26). Whether NR4A2 can impair B cell function

by binding to AP-1 in NR4A2<sup>+</sup> B cells requires further investigation.

*PD-L1 expression significantly correlates with CD20<sup>+</sup> B cell density.* The correlation between PD-L1 and CD20 was examined in order to determine the rationale of combined therapy. The HCC tumor slides were analyzed via IF staining (Fig. 6A) and the data indicated that patients with high PD-L1 expression exhibited high density of B cells as measured by CD20 expression (Fig. 6B). Subsequently, the HCC tumor samples were divided into two groups, namely CD20<sup>high</sup> PD-L1<sup>high</sup> and CD20<sup>low</sup> PD-L1<sup>low</sup> (the thresholds of CD20 and PD-L1 were 6 and 20 cells/mm<sup>2</sup>, respectively). The data indicated that the group with the CD20<sup>high</sup> PD-L1<sup>high</sup> samples exhibited a significant decrease in the percentage of granzyme B<sup>+</sup> CD8<sup>+</sup> TILs compared with the CD20<sup>low</sup> PD-L1<sup>low</sup> group (Fig. 6C). Moreover, the CD20<sup>high</sup> PD-L1<sup>high</sup> group exhibited reduced percentages of both perforin<sup>+</sup> and granzyme B<sup>+</sup> CD4<sup>+</sup> TILs (Fig. 6D). These data indicated that the combined presence of CD20 and PD-L1 could be used as an indicator of compromised antitumor effects in the context of HCC.



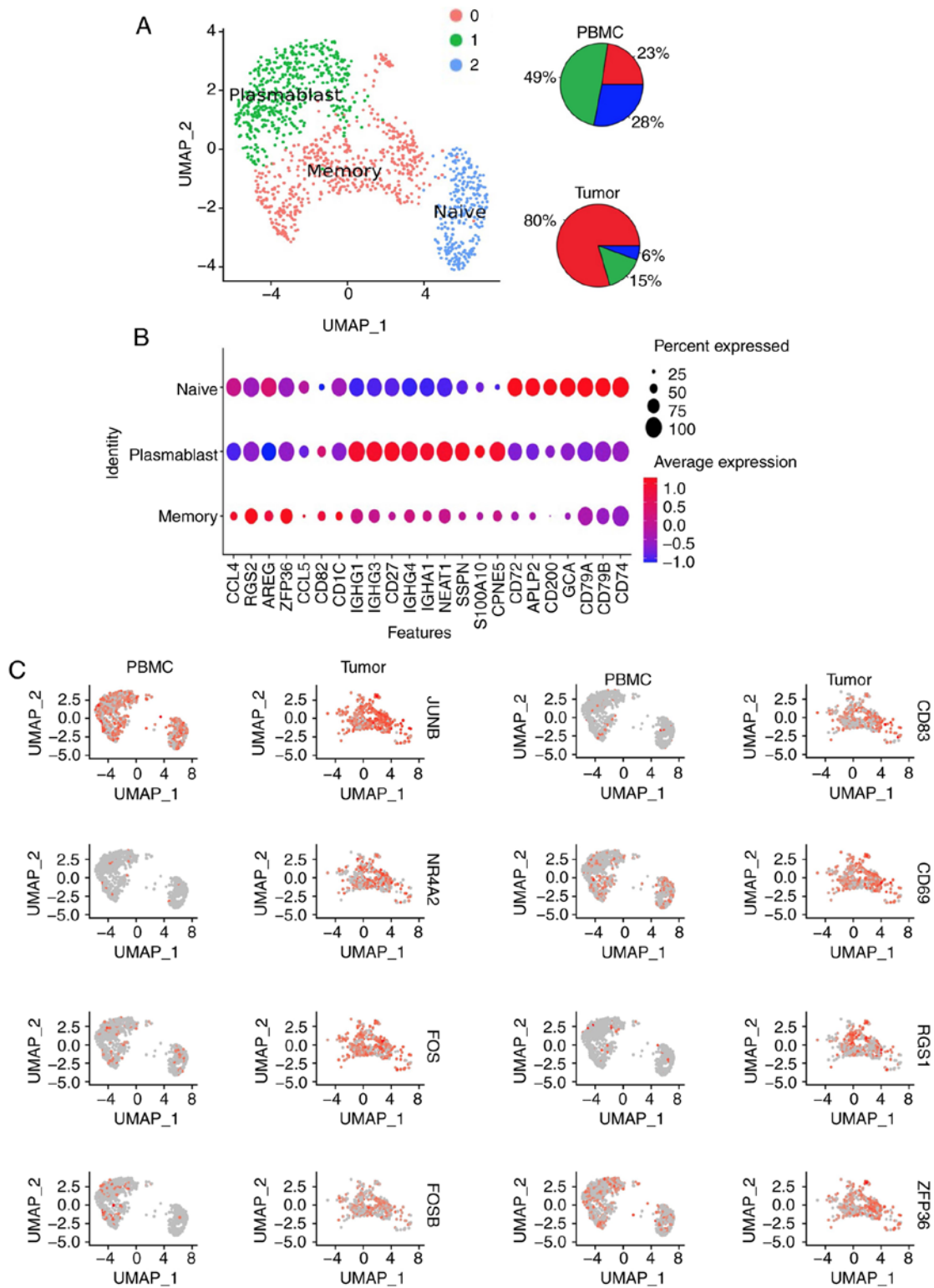


Figure 5. B-TILs indicate higher expression levels of *NR4A2*. (A) UMAP of B cells in tumors and PBMCs indicating three different clusters. Pie charts indicating distribution of each cluster in PBMCs and tumors. (B) Expression of selected genes across the three clusters. (C) UMAP projection split by tissue of origin (PBMCs or tumor) and colored for expression of *JUNB*, *NR4A2*, *FOS*, *FOSB*, *CD83*, *CD69*, *RGS1*, *ZFP36*. Each spot represents one B cell. B-TILs, tumor-infiltrating B cells; NR4A2, nuclear receptor subfamily 4 group A member 2; UMAP, uniform manifold approximation and projection; PBMCs, peripheral blood mononuclear cells.

## Discussion

The present study demonstrated that the density of B cells was increased in the hepatocellular carcinoma (HCC) tumor microenvironment (TME). Patients with high B cell infiltration

had impaired antitumor activity, featured by both CD8<sup>+</sup> T cells and NK cells with compromised ability to express granzyme B and IFN- $\gamma$ . B cells positively were found to be correlated with FOXP3<sup>+</sup> Treg cells. Moreover, PD-L1 expression significantly correlated with the expression of the B cell marker CD20.

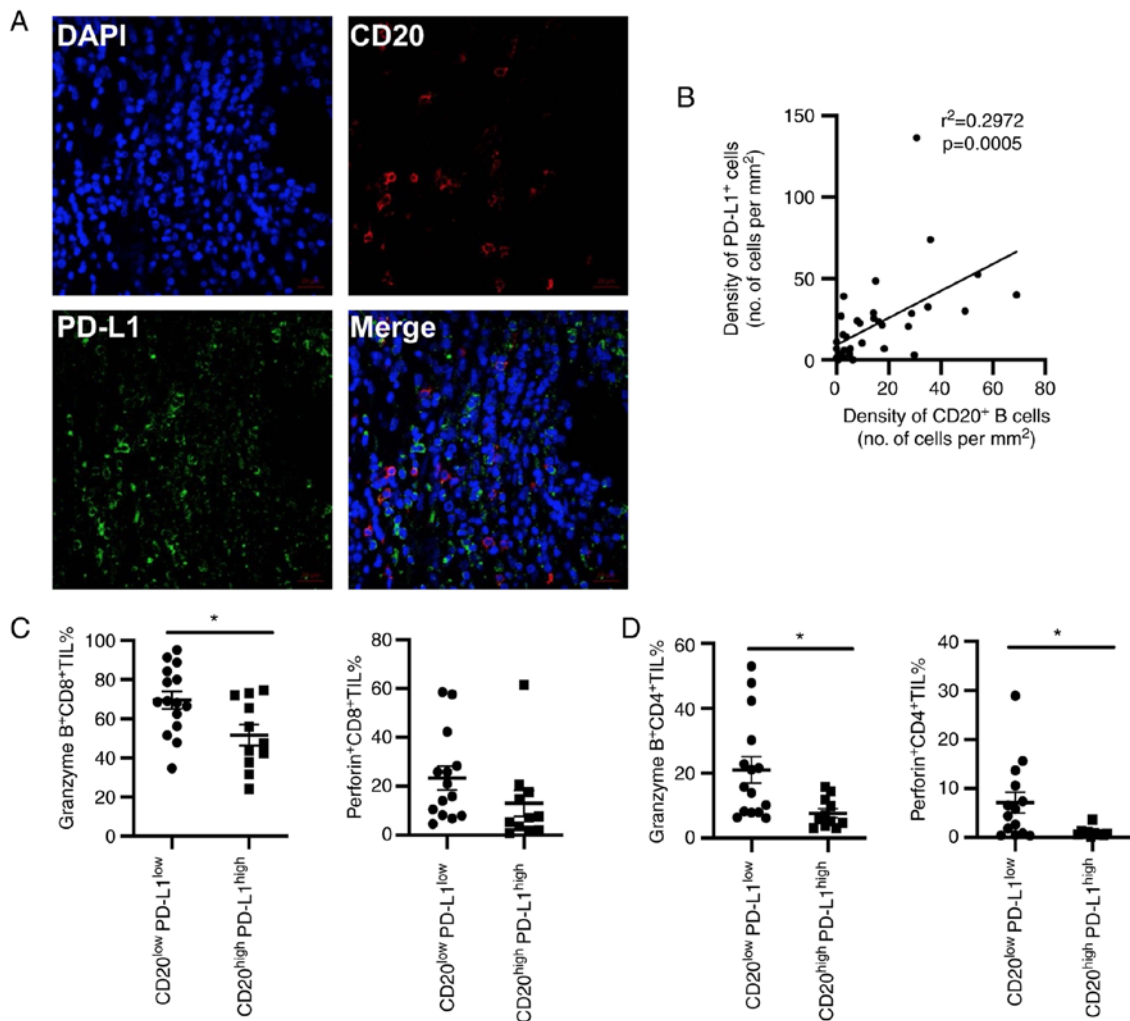


Figure 6. PD-L1<sup>+</sup> cell density is significantly correlated with the density of CD20<sup>+</sup> B cells. (A) Representative images of staining following IF of CD20 and PD-L1 combined with DAPI in tumors. (B) Quantification of PD-L1<sup>+</sup> and CD20<sup>+</sup> B cell densities (number of cells/mm<sup>2</sup>) indicated that the PD-L1 density was positively correlated with CD20<sup>+</sup> B cells (n=37). (C) The CD20<sup>high</sup>PD-L1<sup>high</sup> patient group (n=11) exhibited significantly decreased frequency of granzyme B<sup>+</sup> CD8<sup>+</sup> TILs. (D) The CD20<sup>high</sup>PD-L1<sup>high</sup> patient group (n=11) exhibited significantly decreased frequencies of granzyme B<sup>+</sup> CD4<sup>+</sup> TILs and perforin<sup>+</sup> CD4<sup>+</sup> TILs. \*P<0.05. PD-L1, programmed death ligand-1; TILs, tumor infiltrating lymphocytes; IF, immunofluorescence.

Immune tolerance can result in weak responses towards tumor antigens. The understanding of the underlying mechanisms responsible for immune tolerance can provide strategies to restore an antitumor immune response (27). The identification of the dominant immunosuppressive cells in patients with cancer could serve as an alternative mechanism to overcome immune suppression. It is highly possible that each TME is controlled by a distinct profile of a suppressive cellular compartment (28). The present study indicated that B cells may be a subpopulation of lymphocytes that act as immunosuppressive cells in patients with HCC. In a mouse model of skin carcinogenesis, B cells were required to maintain a chronic inflammation status, which in turn promoted *de novo* carcinogenesis. Therefore, deficiency of B cells reduced infiltration of immune cells in premalignant lesions, while leading to inhibition of carcinoma development (29,30). Furthermore, B cell deficiency was also found to be associated with enhanced antitumor T cell responses in mice with increased IFN- $\gamma$  secretion (31), which was consistent with the findings reported in the present study. In addition, regulatory B (Breg) cells were identified as a leading cause

of HCC progression (32). Breg cells were shown to promote HCC progression by increasing interleukin (IL)-10 and tumor growth factor (TGF)- $\beta$  production via activation of the CD40/CD40 ligand signaling pathway, which resulted in decreased tumor necrosis factor (TNF)- $\alpha$  levels and reduced antitumor immune response (14). Notably, Breg cells were also proposed to suppress T cell antitumor immune response by converting naive CD4<sup>+</sup> T cells to Treg cells in the TME (33). In the present study, a positive correlation between the density of B-TILs and intratumoral Treg cells was noted. However, whether B cells can recruit Treg cells or directly interact with each other requires further investigation.

In the present study, the numbers of both CD8<sup>+</sup> T and Treg cells were positively correlated with B cell density. Garnelo *et al* (16) also reported that the number of B cells was also found to correlate with the number of CD8<sup>+</sup> T cells in HCC using IF staining. Although the number of CD8<sup>+</sup> T cells was positively correlated with that of B cells, their cytotoxic CD8<sup>+</sup> T cell (CTL) function was decreased in patients with high percentage of B cells. One possible explanation could be the increased percentage of Treg cells. Treg

cells play an indispensable role in immune suppression, by suppressing the effector activities of CD4<sup>+</sup> and CD8<sup>+</sup> T cells as well as the function of nature killer (NK) cells (34,35). It has been reported that Treg cells allow CD8<sup>+</sup> T cells to proliferate, while compromising their IFN- $\gamma$  production and cell-mediated cytotoxicity (36). It is interesting to note that in the tertiary lymphoid structure (TLS), CD8<sup>+</sup> T cells were localized close to B cells, and Treg cells were present within the same area. B cells may interact with Treg cells, which in turn inhibit CTL function. The mechanism and pathway through which B cells orchestrate the TME requires further extensive research.

Taken together, the data indicate that B-TILs in HCC are associated with dampened antitumor immunity and may serve as a promising target for immunotherapy.

### Acknowledgements

Not applicable.

### Funding

This research study was supported by grants from Natural Science Foundation of China (31991173 and 31991170), Tsinghua University Spring Breeze Fund (2020Z99CFG008), Tsinghua University-Xiamen Chang Gung Hospital Joint Research Center for Anaphylactic Disease, Youth Program of National Natural Science Foundation of China (81702822) and Bristol-Myers Squibb.

### Availability of data and materials

The RNA-seq datasets analyzed in this study are available in GEPiA2 (<http://gepia2.cancer-pku.cn/#index>). 10x Genomics data were downloaded from GEO dataset (GSE140228, <https://www.ncbi.nlm.nih.gov/geo/query/acc.cgi>) in the published article (21). Data sharing is not applicable to this article as no genomics were generated in this study.

### Authors' contributions

YF performed the majority of the experiments; JL, YS, SX, JHX, LM and WZ performed some of the experiments. LL, JH and HT collected and analyzed the clinical specimens; LL and ZY supervised and analyzed the clinical specimens. XZ performed the single cell data analysis. LN and YF wrote the manuscript; LN designed and supervised the study. All authors reviewed and approved the final manuscript. All authors confirm the accuracy of the data, read and approved the manuscript and agree to be accountable for all aspects of the research in ensuring that the accuracy or integrity of any part of the work are appropriately investigated and resolved.

### Ethics approval and consent to participate

All procedures followed were in accordance with the ethical standards of the responsible committee on human experimentation (The Institutional Review Board at Tsinghua University (Beijing, China) and with the Helsinki Declaration of 1975, as revised in 2000 (5). All studies were approved

by the Medical Ethics Committee at Tsinghua University (approval no. 20180017). Informed consent was obtained from all the subjects in this study.

### Patient consent for publication

Not applicable.

### Competing interests

The authors declare that they have no competing interests. JHX and LM are employees of Bristol Myers Squibb.

### References

1. Ferlay J, Soerjomataram I, Dikshit R, Eser S, Mathers C, Rebelo M, Parkin DM, Forman D and Bray F: Cancer incidence and mortality worldwide: Sources, methods and major patterns in GLOBOCAN 2012. *Int J Cancer* 136: E359-E386, 2015.
2. European Association for the Study of the Liver. Electronic address: easloffice@easloffice.eu; European Association for the Study of the Liver: EASL clinical practice guidelines: Management of hepatocellular carcinoma. *J Hepatol* 69: 182-236, 2018.
3. Zhu RX, Seto WK, Lai CL and Yuen MF: Epidemiology of hepatocellular carcinoma in the asia-pacific region. *Gut Liver* 10: 332-339, 2016.
4. Yang JD and Roberts LR: Hepatocellular carcinoma: A global view. *Nat Rev Gastroenterol Hepatol* 7: 448-458, 2010.
5. Llovet JM, Ricci S, Mazzaferro V, Hilgard P, Gane E, Blanc JF, de Oliveira AC, Santoro A, Raoul JL, Forner A, *et al*: Sorafenib in advanced hepatocellular carcinoma. *N Engl J Med* 359: 378-390, 2008.
6. Buonaguro L, Mauriello A, Cavalluzzo B, Petrizzo A and Tagliamonte M: Immunotherapy in hepatocellular carcinoma. *Ann Hepatol* 18: 291-297, 2019.
7. El-Khoueiry AB, Sangro B, Yau T, Crocenzi TS, Kudo M, Hsu C, Kim TY, Choo SP, Trojan J, Rd THW, *et al*: Nivolumab in patients with advanced hepatocellular carcinoma (CheckMate 040): An open-label, non-comparative, phase 1/2 dose escalation and expansion trial. *Lancet* 389: 2492-2502, 2017.
8. Yarchoan M, Hopkins A and Jaffee EM: Tumor mutational burden and response rate to PD-1 inhibition. *N Engl J Med* 377: 2500-2501, 2017.
9. Leonardi GC, Candido S, Cervello M, Nicolosi D, Raiti F, Travalì S, Spandidos DA and Libra M: The tumor microenvironment in hepatocellular carcinoma (review). *Int J Oncol* 40: 1733-1747, 2012.
10. Shalapour S, Lin XJ, Bastian IN, Brain J, Burt AD, Aksenov AA, Vrbanac AF, Li W, Perkins A, Matsutani T, *et al*: Inflammation-induced IgA<sup>+</sup> cells dismantle anti-liver cancer immunity. *Nature* 551: 340-345, 2017.
11. Ye L, Zhang Q, Cheng Y, Chen X, Wang G, Shi M, Zhang T, Cao Y, Pan H, Zhang L, *et al*: Tumor-derived exosomal HMGB1 fosters hepatocellular carcinoma immune evasion by promoting TIM-1(+) regulatory B cell expansion. *J Immunother Cancer* 6: 145, 2018.
12. Xue H, Lin F, Tan H, Zhu ZQ, Zhang ZY and Zhao L: Overrepresentation of IL-10-expressing B cells suppresses cytotoxic CD4<sup>+</sup> T cell activity in HBV-induced hepatocellular carcinoma. *PLoS One* 11: e0154815, 2016.
13. Schwartz M, Zhang Y and Rosenblatt JD: B cell regulation of the anti-tumor response and role in carcinogenesis. *J Immunother Cancer* 4: 40, 2016.
14. Shaso Y, Lo CM, Ling CC, Liu XB, Ng KTP, Chu AC, Ma YY, Li CX, Fan ST and Man K: Regulatory B cells accelerate hepatocellular carcinoma progression via CD40/CD154 signaling pathway. *Cancer Lett* 355: 264-272, 2014.
15. Zhang Z, Ma L, Goswami S, Ma J, Zheng B, Duan M, Liu L, Zhang L, Shi J, Dong L, *et al*: Landscape of infiltrating B cells and their clinical significance in human hepatocellular carcinoma. *Oncoimmunology* 8: e1571388, 2019.
16. Garnelo M, Tan A, Her Z, Yeong J, Lim CJ, Chen J, Lim KH, Weber A, Chow P, Chung A, *et al*: Interaction between tumour-infiltrating B cells and T cells controls the progression of hepatocellular carcinoma. *Gut* 66: 342-351, 2017.

17. Cabrita R, Lauss M, Sanna A, Donia M, Larsen MS, Mitra S, Johansson I, Phung B, Harbst K, Vallon-Christersson J, *et al*: Tertiary lymphoid structures improve immunotherapy and survival in melanoma. *Nature* 577: 561-565, 2020.
18. Helmink BA, Reddy SM, Gao J, Zhang S, Basar R, Thakur R, Yizhak K, Sade-Feldman M, Blando J, Han G, *et al*: B cells and tertiary lymphoid structures promote immunotherapy response. *Nature* 577: 549-555, 2020.
19. Petitprez F, de Reynies A, Keung EZ, Chen TWW, Sun CM, Calderaro J, Jeng YM, Hsiao LP, Lacroix L, Bougouin A, *et al*: B cells are associated with survival and immunotherapy response in sarcoma. *Nature* 577: 556-560, 2020.
20. Xie S, Huang J, Qiao Q, Zang W, Hong S, Tan H, Dong C, Yang Z and Ni L: Expression of the inhibitory B7 family molecule VISTA in human colorectal carcinoma tumors. *Cancer Immunol Immunother* 67: 1685-1694, 2018.
21. Stuart T, Butler A, Hoffman P, Hafemeister C, Papalexi E, Mauck WM III, Hao Y, Stoeckius M, Smibert P and Satija R: Comprehensive integration of single-cell data. *Cell* 177: 1888-1902.e21, 2019.
22. McInne L and Healy J: UMAP: Uniform Manifold Approximation and Projection for Dimension Reduction. *ArXiv e-prints* 1802.03426, 2018. <https://arxiv.org/abs/1802.03426>.
23. Zhang Q, He Y, Luo N, Patel SJ, Han Y, Gao R, Modak M, Carotta S, Haslinger C, Kind D, *et al*: Landscape and dynamics of single immune cells in hepatocellular carcinoma. *Cell* 179: 829-845 e820, 2019.
24. Li QX, Ke N, Sundaram R and Wong-Staal F: NR4A1, 2, 3-an orphan nuclear hormone receptor family involved in cell apoptosis and carcinogenesis. *Histol Histopathol* 21: 533-540, 2006.
25. Liu X, Wang Y, Lu H, Li J, Yan X, Xiao M, Hao J, Alekseev A, Khong H, Chen T, *et al*: Genome-wide analysis identifies NR4A1 as a key mediator of T cell dysfunction. *Nature* 567: 525-529, 2019.
26. Chen J, Lopez-Moyado IF, Seo H, Lio CWJ, Hempleman LJ, Sekiya T, Yoshimura A, Scott-Browne JP and Rao A: NR4A transcription factors limit CAR T cell function in solid tumours. *Nature* 567: 530-534, 2019.
27. Sakaguchi S, Yamaguchi T, Nomura T and Ono M: Regulatory T cells and immune tolerance. *Cell* 133: 775-787, 2008.
28. Ren Z, Peng H and Fu YX: PD-1 shapes B cells as evildoers in the tumor microenvironment. *Cancer Discov* 6: 477-478, 2016.
29. de Visser KE, Korets LV and Coussens LM: De novo carcinogenesis promoted by chronic inflammation is B lymphocyte dependent. *Cancer Cell* 7: 411-423, 2005.
30. Andreu P, Johansson M, Affara NI, Pucci F, Tan T, Junankar S, Korets L, Lam J, Tawfik D, DeNardo DG, *et al*: FcR $\gamma$  activation regulates inflammation-associated squamous carcinogenesis. *Cancer Cell* 17: 121-134, 2010.
31. Qin Z, Richter G, Schüler T, Ibe S, Cao X and Blankenstein T: B cells inhibit induction of T cell-dependent tumor immunity. *Nat Med* 4: 627-630, 1998.
32. Hetta HF: Regulatory B cells: Key players in hepatocellular carcinoma progression. *Gastroenterology & Hepatology: Open Access* 52016. <https://medcraveonline.com/GHOA/GHOA-05-00136.pdf>
33. DiLillo DJ, Matsushita T and Tedder TF: B10 cells and regulatory B cells balance immune responses during inflammation, autoimmunity, and cancer. *Ann NY Acad Sci* 1183: 38-57, 2010.
34. Shevach EM: From vanilla to 28 flavors: Multiple varieties of T regulatory cells. *Immunity* 25: 195-201, 2006.
35. von Boehmer H: Mechanisms of suppression by suppressor T cells. *Nat Immunol* 6: 338-344, 2005.
36. Lin CY, Graca L, Cobbold SP and Waldmann H: Dominant transplantation tolerance impairs CD8<sup>+</sup> T cell function but not expansion. *Nat Immunol* 3: 1208-1213, 2002.



This work is licensed under a Creative Commons Attribution-NonCommercial-NoDerivatives 4.0 International (CC BY-NC-ND 4.0) License.